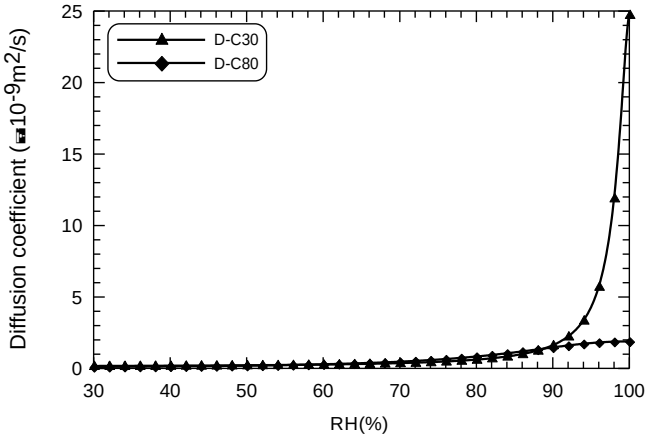

Fig. 3. Water Diffusion Coefficient Used in the Model.

Table 2. Input Parameters Used for Humidity Field Calculation

Concrete	$H_{s,u}$	β	a_m (cm/day)
C30	0.835	3.187	3.0
C80	0.703	1.108	4.1

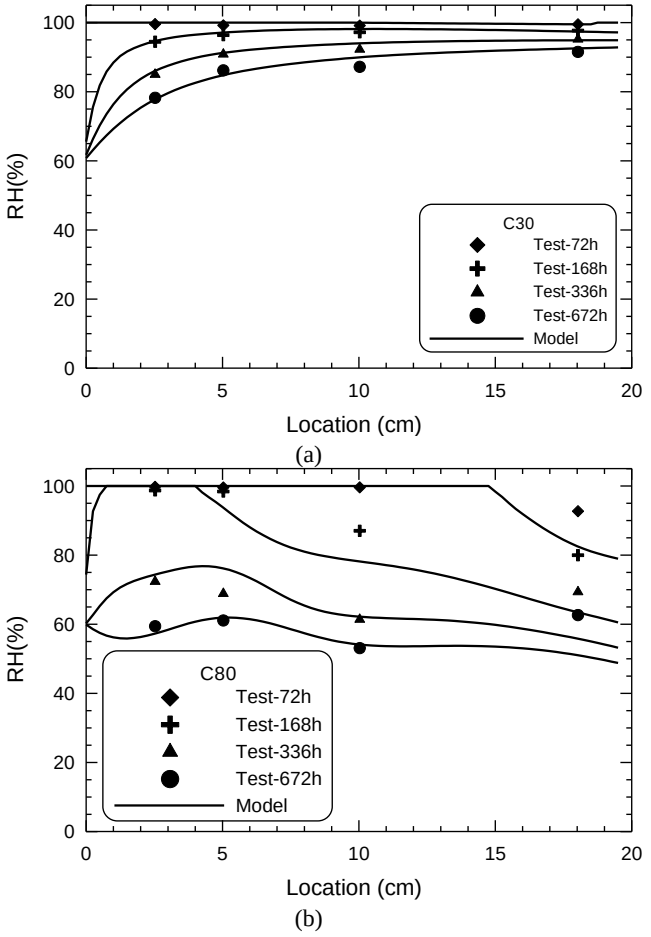

Fig. 4. Comparisons between Predicted Humidity Profile and Experimental Results of C30 (a) and C80 (b) Concrete Slabs.

in spring morning that should influence the development of temperature inside of the slabs. Because the temperature in the slab at early-age is critically needed to calculate the degree of cement hydration, the development of temperature inside the pavement slab was calculated first in the modeling. After the development of temperature inside of concrete pavement is known, the shrinkage strain and stress induced by cement hydration and environmental drying can then be calculated. Regarding the details of the temperature field calculation may refer to author's previous publication [18].

Fig. 5 presents the model results of the development of interior humidity and corresponding shrinkage strain at different places from top to bottom of the pavements made of C30 and C80 concretes respectively. From the results, first we can observe that the development of interior humidity inside of concrete with age obeys the two stage mode, that is a vapor saturated stage with 100% relative humidity (stage I) and a stage with the relative humidity gradually decreasing (stage II). The humidity gradient along the slab depth is significant and is varied with age. Under the condition that the slab surface undergoes drying, the length of stage I increases with the location from the slab top. Second, the shrinkage strain is well related with interior humidity. Within the stage I, a uniform shrinkage strain is expected throughout the slab. By contrast, the shrinkage gradient along the slab depth is quite obvious in the stage II and the maximum and minimum shrinkages occur at slab top and bottom respectively. That is because the humidity gradient starts to occur in this stage and the maximum and minimum humidity reduction appears at slab top and bottom respectively at the moment. The rate of shrinkage progress is gradually reduced from slab top to bottom in this stage, meaning that the effect of surface drying is confined within a certain range.

The distribution of shrinkage strain along the C30 and C80 concrete slab at some typical ages is displayed in Fig. 6. Clearly, shrinkage distribution along the pavement depth is apparently nonlinear. With development of age, the shrinkage gradient is even pronounced. Concrete strength can significantly influence the magnitude of shrinkage strain as well as its distribution in the slab. At a given age and location, the high the concrete strength, the larger the shrinkage strain and the greater the shrinkage gradient. Here we should note that the shrinkage at slab bottom is close to the magnitude of autogenous shrinkage of concrete and at the slab top surface is a result of a combination of autogenous and drying shrinkage. Apparently, high strength concrete will result in high shrinkage strain as well as high shrinkage gradient in concrete members.

Shrinkage Stress in Concrete Pavement

Decomposing of Nonlinearly Shrinkage Strain

A simple illustration of concrete pavement used in modeling is shown in Fig. 7 and assume the length, width and height of the pavement slab are L, W and H respectively. y is the direction perpendicular to the slab length, x is the direction parallel to the slab length. The long ends of the slab are located at $x = 0$ and $x = L$, respectively. z is the direction parallel to the slab depth and the top and bottom ends of the slab are located at $z = H/2$ and $z = -H/2$, respectively. In the case of the top surface of pavement experiences drying, the variation of shrinkage strain is only obvious through the depth of the slab, the influence of slab width and length can then be

To solve this differential equation with boundary conditions that $\partial u / \partial x = \sigma_{a0} / E_c + \varepsilon_a$ at $x = 0$ and $u = \delta_0$ at $x = x_0$, yields:

$$u = \delta_0 + \frac{1}{2}\beta^2\delta_0\left(x^2 - {x_0}^2\right) + \left[\frac{\sigma_{a0}}{E_c} + \varepsilon_a\right]\left(x - x_0\right) \tag{35}$$

Similar to stage I, using Eq. (37) in Eq. (34), the stress in slab within this location can be expressed as

$$\sigma_a = E\beta^2\delta_0 x + \sigma_{a0} \tag{36}$$

For the section of $x_0 < x \le L/2$, the slab/base frictional stress is being developed due to the small slab slippage ($u \le \delta_0$). The procedures used to solve the average displacement and stress fields in stage I can be applied in this section by simply replacing the slab length $L/2$ with $(L/2\text{-}x_0)$ and using a new boundary condition at $x = x_0$ instead of at $x = 0$, i.e. $\partial u / \partial x = \sigma_{a00} / E_c + \varepsilon_a$ at $x = x_0$. σ_{a00} is the thickness average axial stress at $x = x_0$. The displacement and stress fields in this section are given by

$$u = -\frac{1}{\beta}\left[\frac{\sigma_{a00}}{E} + \varepsilon_a\right]\frac{sinh\beta\left(\frac{L}{2} - x\right)}{cosh\beta\left(\frac{L}{2} - x_0\right)} \tag{37}$$

and

$$\sigma_a = -E\varepsilon_a\left[1 - \frac{cosh\beta\left(\frac{L}{2} - x\right)}{cosh\beta\left(\frac{L}{2} - x_0\right)}\right] + \sigma_{a00}\frac{cosh\beta\left(\frac{L}{2} - x\right)}{cosh\beta\left(\frac{L}{2} - x_0\right)} \tag{38}$$

where $\sigma_{a00} = E_c\beta^2\delta_0 x_0 + \sigma_{a0}$. The length x_0 can be numerically determined from Eq. (19) by setting $x = x_0$ and $u = \delta_0$. It should be noted that σ_{a0} may be related to crack bridging law of concrete in general if the slab ends are associated with crack location. The present work is focused on analyzing the development of shrinkage stress in jointed concrete pavements at early-age, so that $\sigma_{a0} = 0$ is used in the examples of analyses.

Shrinkage Stress Resulted from the Linear Strain Component

The general solution for an elastic slab subjected to linear strain profile was given as

$$\begin{aligned} -\frac{\partial^2 w}{\partial x^2} &= \frac{12}{Eh^3}(M_x - \nu M_y) + B \\ -\frac{\partial^2 w}{\partial y^2} &= \frac{12}{Eh^3}(M_y - \nu M_x) + B \end{aligned} \tag{39}$$

where x, y, z are the directions of slab length, width and thickness respectively. w is the displacement in the z-direction. The right side of the above equation represents the total curvature of the slab corresponding to the moment curvature in x and y direction and the curvature due to the linear strain gradient respectively. The stresses produced by the linear strain difference can be obtained by solving above differential equations with appropriate boundary and external restrained conditions. In the present work, research is focus on the solving of shrinkage stresses in concrete pavement in early-age. The slab is normally relatively long and the restrain action along the slab length is significant. So we may assume that $\partial^2 w/\partial x^2 = 0$. Thus from Eq. (39), we have

$$\begin{aligned} M_y &= \frac{Eh^3}{12(1-\nu)}\left[-\frac{\partial^2 w}{\partial x^2} - (1+\nu)B\right] \\ M_x &= \nu M_y - \frac{Eh^3}{12}B \end{aligned} \tag{40}$$

In addition, the moment M_y can be related to the reacting force of base kw by

$$\frac{d^2 M_y}{dy^2} = kw \tag{41}$$

where k is the stiffness of the pavement base. Replace M_y with Eq. (40) in Eq. (41), the general governing equation of w can be rewritten as

$$l^4\frac{\partial^4 w}{\partial y^4} + w = 0 \tag{42}$$

where $l = \left[\frac{Eh^3}{12\left(1-\nu^2\right)k}\right]^{\frac{1}{4}}$. Solve the above differential equation with boundary conditions that $M_y = 0$ and $dM_y/dy = 0$ at $y = \pm W/2$ yields:

$$\begin{aligned} w = w_0\frac{2cosW_l\,coshW_l}{sin2W_l + sinh2W_l}\Bigg[&\left(-tgW_l + tanhW_l\right)cos\frac{y}{l\sqrt{2}}cosh\frac{y}{l\sqrt{2}} \\ &+ \left(tgW_l + tanhW_l\right)sin\frac{y}{l\sqrt{2}}sinh\frac{y}{l\sqrt{2}}\Bigg] \end{aligned} \tag{43}$$

here $w_0 = (1+\nu)Bl^2$, $W_l = W/(l\sqrt{8})$. Thus replace w in Eq. (43) with Eq. (44), we can obtain the expression of the stress distribution in x and y direction through the depth of the slab as

$$\begin{aligned} \sigma_{yz} = 2\sigma_0\Bigg\{1 - \frac{2cosW_l\,coshW_l}{sin2W_l + sinh2W_l}\Bigg[&\left(tgW_l + tanhW_l\right)cos\frac{y}{l\sqrt{2}}cosh\frac{y}{l\sqrt{2}} \\ &+ \left(tgW_l - tanhW_l\right)sin\frac{y}{l\sqrt{2}}sinh\frac{y}{l\sqrt{2}}\Bigg]\Bigg\}\frac{z}{H} \\ \sigma_{xz} = 2\left[\sigma_0 + \nu\left(\sigma_{yz} - \sigma_0\right)\right]\frac{z}{H} \end{aligned} \tag{44}$$

where $\sigma_0 = EBH/2(1-\nu)$, which is the stress as slab length and width are infinite and the deformation produced by the shrinkage differences is fully restrained. The maximum stress produced by the linear shrinkage component will occur at the section with $y = 0$ in the direction of x-axial. The stress distribution in the section of $y = 0$ along x-direction, σ_{xz} can be expressed as

$$\sigma_{xz} = 2\sigma_0 [1-\nu(1-C_y)] \frac{z}{H} \quad (45)$$

where $C_y = 1 - \frac{2\cos W_l \cosh W_l}{\sin 2W_l + \sinh 2W_l}\left(tgW_l + \tanh W_l\right)$, that is a function of slab width and depth as well as stiffness of slab and the supporting base.

Shrinkage Stress Resulted from the Nonlinear Component

According to the assumption that the cross section of the pavement remains plane under the action of shrinkage strain, the stress caused by the nonlinear component can be calculated by

$$\sigma_n = -\frac{E}{1-\nu}(\varepsilon_w - A - Bz) \quad (46)$$

Thus, the total shrinkage stresses produced by such nonlinear shrinkage strain in the slab can be obtained by summing the three stress components together as:

$$\sigma_t = \sigma_a + \sigma_l + \sigma_n \quad (47)$$

Creep Correction on the Shrinkage Stresses

Creep of concrete leads to the stress relaxation. To correctly calculate the shrinkage stresses in concrete pavement, the effect of concrete creep must be taken into account. In the present paper, a method given by Zhu [19] is used to correct the effect of concrete creep. Assume the initial stress without considering of the effect of creep at time t_0 is equal to σ_0. After the time period (t-t_0), the stress becomes $\sigma(t)$ due to the action of creep. Now assume the time interval (t-t_0) is divided into n sections, Δt_1, Δt_2, Δt_3,…Δt_i,…Δt_n, and the stress increment in each time section is $\Delta \sigma_1$, $\Delta \sigma_2$, $\Delta \sigma_3$,…$\Delta \sigma_i$,…$\Delta \sigma_n$. Thus the stress at time t can then be given as:

$$\sigma(t) = \sigma(t_0) + \sum_{i=1}^{n} \Delta\sigma_i(t_i) \quad (48)$$

where $t_i = t_0 + \sum_{i=1}^{n-i} \Delta t_i$. As taking the concrete creep into account, the stress with an initial value of $\sigma(t_0)$ after the time period (t-t_0) can be calculated by:

$$\sigma(t,t_0) = \sigma(t_0)\left[1 - \frac{\varphi(t,t_0)}{1+\varphi(t,t_0)}\right] \quad (49)$$

where $\varphi(t,t_0)$ is called creep coefficient and can be calculated by Bazant et al [21]:

$$\varphi(t,t_0) = \varphi_1 t_0^{-d}(t-t_0)^p \quad (50)$$

where φ_1, d and p are material parameters. In present paper, $\varphi_1 = 0.9$, $d = 0.32$, $p = 0.32$ are used in the model calculation according to the reference [21]. Thus, the shrinkage stresses as considering the effect of concrete creep can be given as:

Table 3. Frictional Restraint Characteristics of Typical Base.

Base Type	τ_0 (MPa)	δ_0 (mm)	k(GPa)
Cement Stabilized	0.106	0.025	81

$$\sigma(t,t_i) = \sigma(t_0)\left[1 - \frac{\varphi(t,t_0)}{1+\varphi(t,t_0)}\right] + \sum_{i=1}^{n} \Delta\sigma(t_i)\left[1 - \frac{\varphi(t,t_i)}{1+\varphi(t,t_i)}\right] \quad (51)$$

Analyses of Shrinkage Stress in Concrete Pavement at Early-Ages

As an example of the model application, the shrinkage stress in concrete pavements made of C30 and C80 concrete respectively is calculated. The cement stabilized base is assumed and the friction restraint parameters between slab and base as well as the stiffness of base used in the model are list in Table 3. For modeling, it is assumed that the dimension of the slab is 10 meters in length, 4 meters in width and 0.25 meters in thickness. The shrinkage stress calculation is based on above prediction of shrinkage strain (ε_w).

Fig. 8(a) shows the development of the total shrinkage stress in the middle section of C30 concrete slab with age, where the effects of location from top to bottom are displayed. Fig. 8(b) shows the development of the total shrinkage stress at slab top with age, where the effect of location in length direction is presented. Fig. 9 show analogous results of C80 concrete pavement. From these results, we can see that shrinkage stress occurred in concrete pavement under the condition that the slab top experiences drying are function of construction age, location in both length and depth directions. First, for given age and surface drying condition, the shrinkage stress increases with location in length direction and the maximum stress achieve at the center of the slab. Such behavior is the result of interfacial friction between slab and supporting base occurred during concrete shrinking. Therefore, the variation of shrinkage stress with location in length direction is only controlled by the average shrinkage strain component, A, which in turn is governed by the overall shrinkage distribution in the slab and its variation with age as well. Second, for given age and length location, the variation of shrinkage stress along slab depth is principally controlled by the shrinkage gradient. The linear and nonlinear strain components are the main contributor to such stress variation through the depth. Third, shrinkage stresses along the pavement depth is nonlinearly distributed. The stress gradient is more and more pronounced with time going. Fourth, concrete strength can significantly influence the magnitude of shrinkage stress, as well as its distribution in the slab. At a given age and location, the higher the concrete strength, the larger the shrinkage stress and the greater the stress gradient. In addition, we may be noted also from Fig. 9 that the influencing scope of surface drying on the shrinkage stress is a function of concrete strength and age. Influencing depth increases with age for all three kinds of concretes. In the view of durability design of concrete structures, all above characteristics related to shrinkage stress occurred in concrete members should considerably be taken into account.

Conclusions

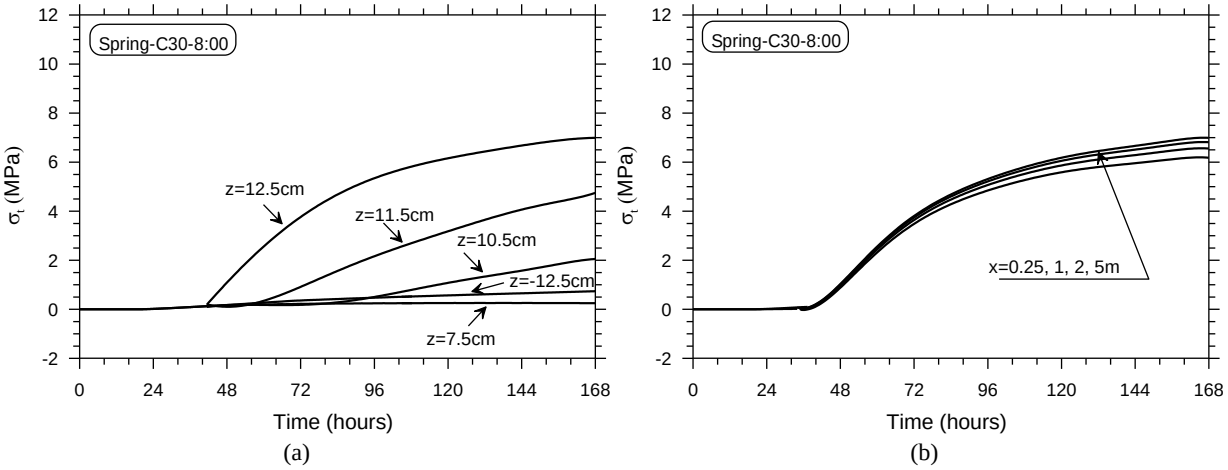

Fig. 8. Development of Shrinkage Stress in C30 Concrete Pavement, (a) Showing the Effect of Location in Depth and (b) Showing the Effect of Location in Length.

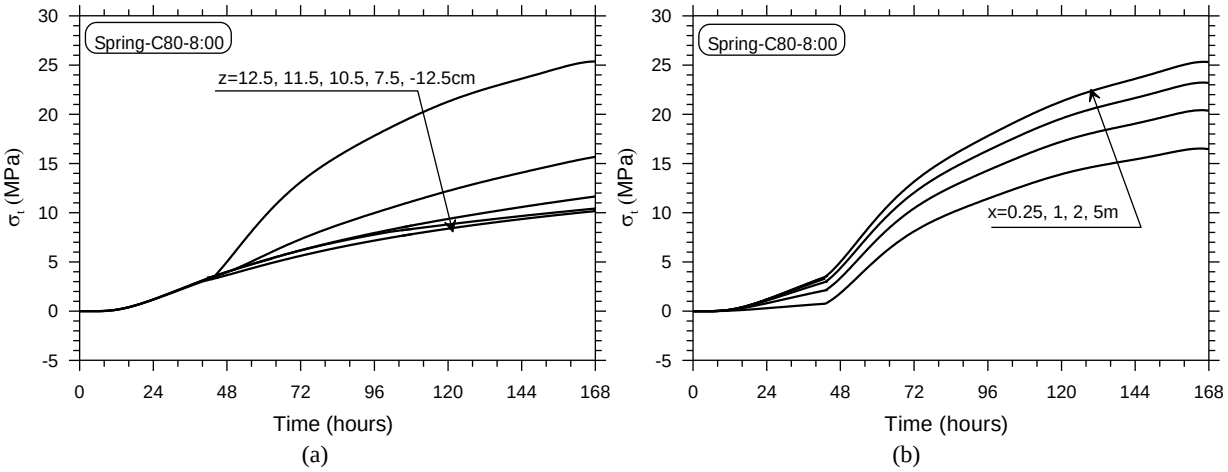

Fig. 9. Development of Shrinkage Stress in C80 Concrete Pavement with Consideration of Creep, (a) Showing the Effect of Location in Depth and (b) Showing the Effect of Location in Length.

In this paper, an integrative model for shrinkage strain and stress in concrete pavements at early-age from concrete cast are simulated and analyzed. The model results show that the progress of internal humidity inside of pavement since concrete cast obeys two stage mode, that is a vapor saturated stage with 100% relative humidity (stage I) and a stage with the relative humidity gradually decreasing (stage II). Within stage I, a uniform shrinkage strain and stress is expected throughout the slab. By contrast, shrinkage gradient along the slab depth is quite significant in stage II and the maximum and minimum shrinkage strain and stress occur at slab top and bottom respectively. The distribution of shrinkage strain and stress along the pavement depth is nonlinear and the nonlinearity is strong close to the drying area. Concrete strength can significantly influence the magnitude of shrinkage strain and stress, as well as their distribution in the slab.

Acknowledgements

This work has been supported by grants from the National Science Foundation of China (No. 50978143, 51178248) to Tsinghua University.

References

1. Ayano, T., Wittmann, F.H. (2002). Drying, Moisture Distribution, and Shrinkage of Cement-based Materials. *Materials and Structures*, 35(247), pp.134-140.
2. Bissonnette B, Pierre P, Pigeon M. (1999). Influence of Key Parameters on Drying Shrinkage of Cementitious Materials. *Cement and Concrete Research*, 29(10), pp. 1655-1662.
3. Zhang, J., Hou, D. W. and Sun, W. (2010). Experimental Study on the Relationship Between Shrinkage and Interior Humidity of Concrete at Early Age. *Magazine of Concrete Research*, 62(3) pp. 191-199.
4. Zhang, J., Hou, D. and Chen, H. (2011). Experimental and Theoretical Studies on Shrinkage of Concrete at Early-ages. *ASCE Journal of Materials in Civil Engineering*, 23(3), pp. 312-320.
5. Zhang, J., Hou, D. and Han Y. (2011). Micromechanical Model of Autogenous and Drying Shrinkages of Concrete. *Building and Construction Materials*, 29(3), pp. 230-240.
6. Powers, T.C. and Brownyard, T.L. (1946). Studies of the Physical Properties of Hardened Portland Cement Paste. *Journal of America Concrete Institute*. 43, Bulletin 22,

Research Laboratories of the Portland Cement Association, Chicago.
7. Jensen, O.M. and Hansen, P.F. (2001). Water-entrained Cement-based Materials: I. Principles and Theoretical Background. *Cement and Concrete Research*, 31(5), pp. 647-654.
8. Rastrup, E. (1954). Heat of Hydration. *Magazine of Concrete Research*, 6(17), pp. 127-140.
9. Kjellsen, K. and Detwiler, R.J. (1993). Later-age Strength Prediction by a Modified Maturity Model. *ACI Materials Journal*, 90(3), pp. 220-227.
10. Chanvillard, G. and Daloia, L. (1997). Concrete Strength Estimation at Early Age: Modification of the Method of Equivalent Age. *ACI Materials Journal*, 94(6), pp. 220-227.
11. Kim, J.K. (2001). Estimation of Compressive Strength by a New Apparent Activation Energy Function. *Cement and Concrete Research*, 31(2), pp. 217-225.
12. Pane, I. and Hansen, W. (2002). Concrete Hydration and Mechanical Properties under Nonisothermal Conditions. *ACI Materials Journal*, 99(6), pp. 534-422.
13. Zhang, J., Qi, K. and Huang, Y. (2009). Calculation of Moisture Distribution in Early-age Concrete. *ASCE Journal of Engineering Mechanics*, 135(8), pp. 871-880.
14. Akita, H., Fujiwara, T. and Ozaka, Y. (1997). A practical procedure for the analysis of moisture transfer within concrete due to drying. *Magazine of Concrete Research*, 49(179), pp. 129-137.
15. Bazant, Z.P., and Najjar, L.J. (1972). Nonlinear Water Diffusion in Nonsaturated Concrete. *Materials and Structures*, 5(25), pp. 3-20.
16. Nilsson, L.O. (2002). Long-term Moisture Transport in High Performance Concrete. *Materials and Structures*, 35, pp. 641-649.
17. Zhang, J., Hou, D. Gao Y. and Sun, W. (2011). Determination of Moisture Diffusion Coefficient of Concrete at Early-age from Interior Humidity Measurements. *Drying Technology*, 29(6), pp. 689-696.
18. Hou, D. Zhang, J. and Gao, Y. (2012). Simulation of temperature field of concrete pavement at early age. *Engineering Mechanics*, 29(6), pp.151-159 (in Chinese).
19. Zhu, B.F. (1999). *Thermal Stress and Temperature Control in Mass Concrete*. Electric Power Publishing House, Beijing, China (in Chinese).
20. Zhang, J. and Li, V.C. (2001). Influence of Supporting Base Characteristics on the Shrinkage Induced Stresses in Concrete Pavements. *ASCE Journal of Transportation Engineering*, 127(6), pp. 455-462.
21. Bazant, Z.P. and Panula, L. (1978). Practical Prediction of Time Dependent Deformation of Concrete. *Materials and Structures*, Part I and II, 11(65), pp. 307-328; parts III and IV, 11(66), pp.415-434; Parts V and VI, 12(69), pp. 169-173.